

Article

Crystal Structure of Moganite and Its Anisotropic Atomic Displacement Parameters Determined by Synchrotron X-ray Diffraction and X-ray/Neutron Pair Distribution Function Analyses

Seungyeol Lee ^{1,2,3} , Huifang Xu ^{1,*} , Hongwu Xu ⁴ and Joerg Neuefeind ⁵¹ Department of Geoscience, University of Wisconsin–Madison, Madison, WI 53706, USA; slee2@lpi.usra.edu² USRA Lunar and Planetary Institute, 3600 Bay Area Boulevard, Houston, TX 77058, USA³ ARES, NASA Johnson Space Center, 2101 NASA Parkway, Houston, TX 77058, USA⁴ Earth and Environmental Sciences Division, Los Alamos National Laboratory, Los Alamos, NM 87545, USA; hxu@lanl.gov⁵ Neutron Scattering Division, Oak Ridge National Laboratory, Oak Ridge, TN 37831, USA; neuefeindjc@ornl.gov

* Correspondence: hfxu@geology.wisc.edu; Tel.: +1-608-265-5887



check for updates

Citation: Lee, S.; Xu, H.; Xu, H.; Neuefeind, J. Crystal Structure of Moganite and Its Anisotropic Atomic Displacement Parameters Determined by Synchrotron X-ray Diffraction and X-ray/Neutron Pair Distribution Function Analyses. *Minerals* **2021**, *11*, 272. <https://doi.org/10.3390/min11030272>

Academic Editors:

Emanuela Schingaro and
Hans-Rudolf Wenk

Received: 27 January 2021

Accepted: 4 March 2021

Published: 7 March 2021

Publisher's Note: MDPI stays neutral with regard to jurisdictional claims in published maps and institutional affiliations.



Copyright: © 2021 by the authors. Licensee MDPI, Basel, Switzerland. This article is an open access article distributed under the terms and conditions of the Creative Commons Attribution (CC BY) license (<https://creativecommons.org/licenses/by/4.0/>).

Abstract: The crystal structure of moganite from the Mogán formation on Gran Canaria has been re-investigated using high-resolution synchrotron X-ray diffraction (XRD) and X-ray/neutron pair distribution function (PDF) analyses. Our study for the first time reports the anisotropic atomic displacement parameters (ADPs) of a natural moganite. Rietveld analysis of synchrotron XRD data determined the crystal structure of moganite with the space group $I2/a$. The refined unit-cell parameters are $a = 8.7363(8)$, $b = 4.8688(5)$, $c = 10.7203(9)$ Å, and $\beta = 90.212(4)^\circ$. The ADPs of Si and O in moganite were obtained from X-ray and neutron PDF analyses. The shapes and orientations of the anisotropic ellipsoids determined from X-ray and neutron measurements are similar. The anisotropic ellipsoids for O extend along planes perpendicular to the Si-Si axis of corner-sharing SiO_4 tetrahedra, suggesting precession-like movement. Neutron PDF result confirms the occurrence of OH over some of the tetrahedral sites. We postulate that moganite nanomineral is stable with respect to quartz in hypersaline water. The ADPs of moganite show a similar trend as those of quartz determined by single-crystal XRD. In short, the combined methods can provide high-quality structural parameters of moganite nanomineral, including its ADPs and extra OH position at the surface. This approach can be used as an alternative means for solving the structures of crystals that are not large enough for single-crystal XRD measurements, such as fine-grained and nanocrystalline minerals formed in various geological environments.

Keywords: moganite; quartz; anisotropic atomic displacement parameter; synchrotron X-ray diffraction; neutron scattering; pair distribution function analysis; Rietveld refinement; nanomineral

1. Introduction

Moganite (CNMMN no. 99–035) is a silica polymorph that takes the name from its locality: the Mogán formation on southern Gran Canaria in the Canary Islands, first described by Flörke et al. (1976) [1]. Moganite has been observed ubiquitously in silica sinters, volcanic rocks, carbonate turbidites and deep-sea sediments around the world and is used as an important indicator for evaporitic paleoenvironments [1–7]. It has been identified as a common constituent in silica varieties such as chert, agate, flint, and chalcedony and commonly coexists with fine-grained quartz [1,2,8–10]. Moganite is a metastable phase that eventually transforms to quartz or dissolves preferentially during diagenesis and aging [5,11,12]. Recently, moganite has been discovered in a lunar meteorite in the form of nanocrystalline aggregates in KREEP (high potassium, rare-earth element,

and phosphorus), indicating the possibility of the presence of abundant water resources under the Moon's regolith [13].

The crystal structure of moganite was described as the alternating stacking of left- and right-handed α -quartz domains bounded by {101} planes, corresponding to Brazil-law twinning of α -quartz at the unit-cell scale [3,14]. The same structure was observed in high-pressure phases of PON [15] and AlPO_4 [16]. Moganite exhibits a displacive phase transition from monoclinic ($I2/a$) to orthorhombic ($Imab$) when heated to 297 °C [14] and transforms to cristobalite above 900 °C [3,8]. The presence of water in moganite has been reported in several studies [12,17–19], suggesting that water mainly occurs as free water and silanol species (Si–OH).

Since moganite nanocrystals are not large enough for single-crystal X-ray or neutron diffraction measurements, its detailed structural determination is challenging [4,20]. Moreover, moganite is always intergrown with fine-grained quartz [2,20,21]. Thus, the application of advanced powder diffraction analysis is essential to solving the structure of natural moganite. In this work, we studied the crystal structure of moganite using synchrotron X-ray diffraction (XRD) and X-ray/neutron pair distribution function (PDF) analyses. The combined approach, employing third-generation synchrotron radiation, is a powerful means for studying fine-grained or nanocrystalline mineral systems [22–24]. While high-resolution XRD and neutron diffraction can determine the average structure [25–28], X-ray/neutron PDF analysis is particularly sensitive in determining the local structure including atomic anisotropic displacement parameters (ADPs) [22–29]. ADPs reflect atomic movements and the possible static displacement disorder of atoms in the structure [30]. This study reports for the first time the ADPs of natural moganite.

2. Materials and Methods

Moganite samples were collected from unconsolidated powders that form rinds around a chert found within the ignimbrite lava flows of the Mogán formation on Gran Canaria, Spain (Figure S1). The white powder in the sample was the main subject of our study. Moganite from Mogán formation has been extensively studied using various techniques such as XRD, electron probe microanalysis (EPMA), infrared spectroscopy and nuclear magnetic resonance spectroscopy [1,3,14,20,31].

EPMA specimens were prepared as carbon coated thin sections. EPMA measurements with wavelength dispersive spectrometers (WDS) were made with a CAMECA SXFive FEG electron microprobe using 20 kV and 15 nA beam current in the Geoscience Department of the University of Wisconsin–Madison. TEM specimens were prepared by depositing drops of moganite suspension on carbon-coated TEM Cu grids. High-angle annular-dark-field images, TEM images and their selected-area electron diffraction (SAED) patterns were obtained using FEI Titan 80–200 and JEOL 2010 microscopes operated at 200 keV.

High-resolution X-ray powder diffraction patterns were collected at beamline 11-BM, Advanced Photon Source (APS), Argonne National Laboratory, using a wavelength of 0.412836 Å. The finely ground powders from the moganite sample were placed into a 0.8 mm diameter polyimide tube. The XRD measurement was calibrated using a LaB_6 standard. The crystal structures and mineral phase ratios in the sample were determined using the Rietveld method with the GSASII software [32]. The structures of moganite [14], quartz [33], gypsum [34] and halite [35] were used as the initial structures for the Rietveld refinement. The crystallite sizes were determined by full width at half maximum (FWHM) and integral breadth from whole peak profile.

Synchrotron X-ray PDF experiments were conducted using a wavelength of 0.24152 Å on beamline 17-BM at the APS, Argonne National Laboratory. The moganite sample was placed into a polyimide tube with a 1 mm diameter. An amorphous silicon area detector was used to collect two-dimensional diffraction patterns in the transmission geometry. Each single exposure on the detector was set to 1 s and was repeated 300 times, totaling a collection time of 300 s. The distances between the sample and the detector and the center positions of the beams were calibrated using a LaB_6 standard. For background removal,

diffraction data of the empty polyimide tube were collected using the same exposure times. GSAS-II software was used to convert diffraction images to conventional 1-D profiles (i.e., intensity versus wave vector Q). The data obtained up to a Q_{\max} of 19.6 \AA^{-1} were then converted into PDF patterns using PdfGetX3 [36]. The instrumental resolution parameters of Q_{damp} and Q_{broad} were 0.045 and 0.069 \AA^{-1} , respectively. PDF fitting and refinement were performed using the PDFGui program [37].

Neutron PDF measurements were performed on the NOMAD instrument (BL-1B beamline) at the Spallation Neutron Source (SNS), Oak Ridge National Laboratory. The powder sample was loaded into a 3 mm diameter quartz capillary. The neutron PDF pattern was calculated with the NOMAD data reduction software by the Fourier transformation of the structure function $S(Q)$. The data obtained up to a Q_{\max} of 31.4 \AA^{-1} were transformed into PDF patterns using the PDFgetN program [38]. The instrumental resolution parameters of Q_{damp} and Q_{broad} were 0.01766 and 0.01918 \AA^{-1} , respectively. PDFGui software was used for fitting the neutron PDF data.

3. Results

3.1. High-Resolution Synchrotron XRD

High-resolution synchrotron XRD reveals the presence of the (011) and (200) peaks of moganite adjacent to the (010) peak of quartz (Figure 1). The sample contains moganite 75.3(5) wt.%, quartz 14.2(3) wt.%, gypsum 6.6(2) wt.% and halite 3.7(2) wt.% determined by Rietveld refinement (Figure 1). Previous studies also showed the occurrence of moganite (~65–85 wt. %), quartz, gypsum and halite in similar samples from the Mogán formation [2,19]. The crystallite sizes are estimated as moganite (68.6 nm), quartz (95.5 nm), gypsum (473.1 nm) and halite (749.5 nm) from the XRD pattern. The refined unit cell parameters, atomic coordinates and isotropic displacement parameters (U_{iso}) of these phases are presented in Table 1. Moganite has unit cell parameters of $a = 8.7363(8)$, $b = 4.8688(5)$, $c = 10.7203(9) \text{ \AA}$, and $\beta = 90.212(4)^\circ$ with space group $I2/a$ (which follows the non-conventional setting to maintain the relationship with the trigonal quartz cell). The refined structure of moganite is well matched with the reported structures [3,14]. The calculated density of moganite (2.63 g/cm^3) is slightly lower than that of quartz (2.65 g/cm^3). The refined structure of nanocrystalline quartz has a slightly larger unit cell than reported (Table 1). The refined unit cell parameters of gypsum are similar to the previously reported values [34,35]. Impurities may influence the unit cell parameters of halite and gypsum.

3.2. EPMA

The major elements of moganite areas show almost pure silica with Na, K, Mg, Ca, Al and Fe impurities at trace levels (Table 2). The EPMA results of moganite also reveal a water content of 3.13–5.31 wt.% by directly analyzing O using EPMA and assigning the excessive O to H_2O . Thus, its chemical formula is $\text{SiO}_2 \cdot 0.145\text{H}_2\text{O}$ based on the average values listed in Table 2. Weight loss of approximately 5% of almost pure moganite was suggested by thermogravimetric analysis from 298 to 983 K [5]. Infrared spectra of moganite indicate that ~2–3 wt.% of water is not a constituent of the structure [1,3,17,19]. The water in moganite is mainly in the form of silanol species (Si-OH) and free water, and the ratio $\text{H}_2\text{O}_{\text{SiOH}}/\text{H}_2\text{O}_{\text{free}}$ is approximately 1.2 [19]. Moganite also contains a CO_2 content of ~0.1–1.0 wt.% with a minor component of CO identified by mass spectroscopy [8,19].

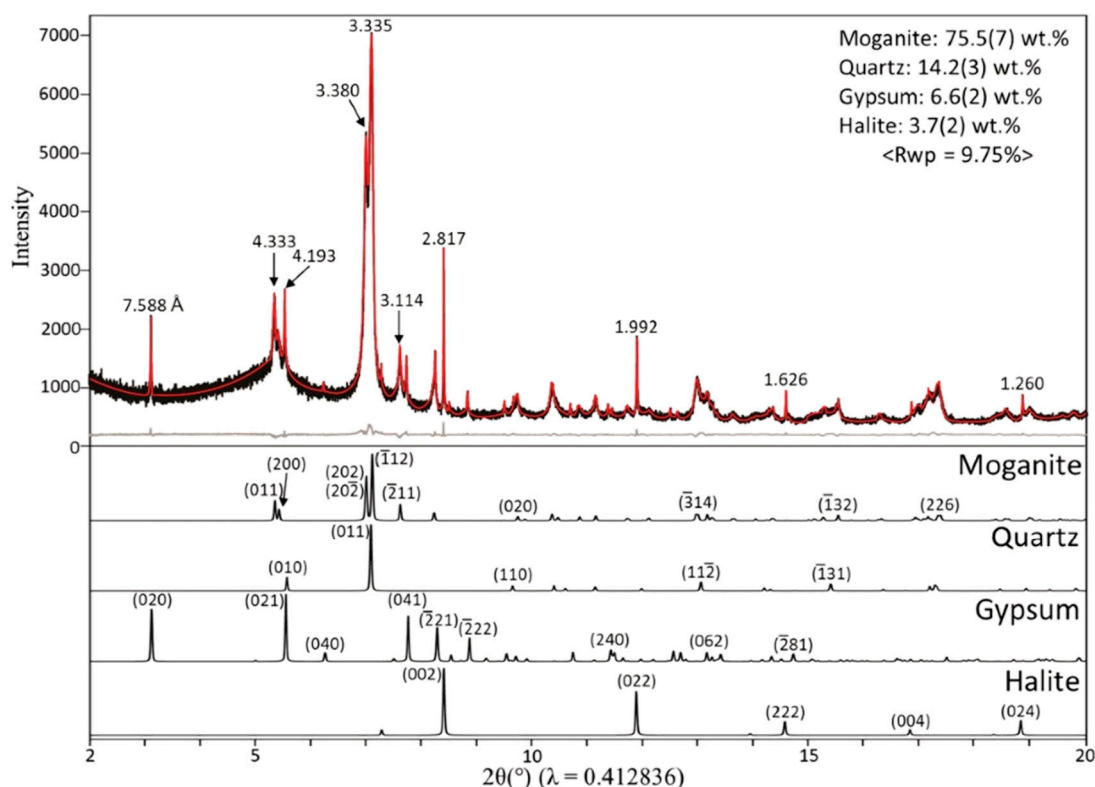


Figure 1. Experimental and calculated synchrotron X-ray diffraction (XRD) patterns (overlapped black and red lines) of the studied sample consisting of moganite, quartz, gypsum and halite. The weight percentages of the mineral phases were determined using the Rietveld method. The residue (grey line) between the experimental data and calculated profile is shown below the XRD pattern.

Table 1. Unit-cell parameters, atomic coordinates and thermal displacement parameters (U_{iso}) of moganite, quartz, halite and gypsum determined by Rietveld refinement (Figure 1).

| Moganite (Space Group $I2/a$) | | | | |
|-----------------------------------------------------------------------------------------------------------------------|------------|-----------|------------|------------------------------|
| Atom | x | y | z | U_{iso} (\AA^2) |
| Si1 | 0.2500 | 0.9731(7) | 0.0000 | 0.0129(5) |
| Si2 | 0.0089(4) | 0.2512(5) | 0.1663(4) | 0.0173(5) |
| O1 | 0.9773(7) | 0.0651(7) | 0.2873(4) | 0.0184(6) |
| O2 | 0.1683(4) | 0.1710(4) | 0.1004(4) | 0.0195(6) |
| O3 | 0.8696(7) | 0.2302(4) | 0.0676(5) | 0.0201(6) |
| Lattice parameters: $a = 8.7363(8)$, $b = 4.8688(5)$, $c = 10.7203(17)$ \AA and $\beta = 90.212(13)^\circ$ | | | | |
| Quartz (Space Group $P3_221$) | | | | |
| Atom | x | y | z | U_{iso} (\AA^2) |
| Si | 0.4690(5) | 0.0000 | 0.0000 | 0.0084(3) |
| O | 0.4134(6) | 0.2671(4) | 0.1192(3) | 0.0142(3) |
| Lattice parameters: $a = 4.9156(4)$ and $c = 5.4052(4)$ \AA | | | | |
| Halite (Space Group $Fm\bar{3}m$) | | | | |
| Atom | x | y | z | U_{iso} (\AA^2) |
| Na | 0.0000 | 0.0000 | 0.0000 | 0.0237(2) |
| Cl | 0.5000 | 0.5000 | 0.5000 | 0.0193(2) |
| Lattice parameters: $a = 5.6338(7)$ \AA | | | | |
| Gypsum (Space Group $C2/c$) | | | | |
| Atom | x | y | z | U_{iso} (\AA^2) |
| Ca | 0.0000 | 0.1693(4) | 0.2500 | 0.0111(3) |
| S | 0.0000 | 0.3289(5) | 0.7500 | 0.0095(3) |
| O1 | 0.0834(2) | 0.2729(4) | 0.5918(7) | 0.0152(5) |
| O2 | 0.2015(5) | 0.3831(6) | 0.9149(6) | 0.0149(5) |
| Ow | -0.2106(7) | 0.0665(4) | -0.0808(6) | 0.0236(6) |
| Lattice parameters: $a = 6.2820(6)$, $b = 15.175(9)$, $c = 5.673(5)$ \AA and $\beta = 117.51(2)^\circ$ | | | | |

Note: Unit cell parameters of reported quartz, $a = 4.914$ \AA , $c = 5.405$ \AA [33], $a = 4.91344$ \AA and $c = 5.40512$ \AA [39].

Table 2. Major element compositions of moganite obtained by electron probe microanalysis (EPMA).

| | (1) | (2) | (3) | (4) | (5) | (6) | Average |
|--------------------------------|-------|-------|-------|-------|-------|-------|---------|
| Si (wt.%) | 44.03 | 43.86 | 43.46 | 43.59 | 43.83 | 43.85 | 43.77 |
| O | 52.97 | 53.08 | 53.86 | 53.80 | 54.67 | 53.92 | 53.72 |
| Na | 0.06 | 0.01 | 0.02 | 0.04 | 0.05 | 0.03 | 0.03 |
| K | 0.02 | 0.01 | 0.00 | 0.01 | 0.02 | 0.00 | 0.01 |
| Mg | 0.01 | 0.00 | 0.01 | 0.01 | 0.01 | 0.01 | 0.01 |
| Ca | 0.02 | 0.03 | 0.02 | 0.03 | 0.01 | 0.02 | 0.02 |
| Al | 0.01 | 0.03 | 0.02 | 0.03 | 0.00 | 0.01 | 0.02 |
| Fe | 0.05 | 0.09 | 0.05 | 0.01 | 0.03 | 0.04 | 0.05 |
| Total | 97.17 | 97.11 | 97.43 | 97.51 | 98.62 | 97.89 | 97.62 |
| SiO ₂ (wt.%) | 94.20 | 93.83 | 92.97 | 93.26 | 93.76 | 93.80 | 93.64 |
| Na ₂ O | 0.08 | 0.01 | 0.03 | 0.05 | 0.06 | 0.04 | 0.04 |
| K ₂ O | 0.02 | 0.01 | 0.00 | 0.02 | 0.03 | 0.00 | 0.01 |
| MgO | 0.01 | 0.00 | 0.01 | 0.01 | 0.01 | 0.02 | 0.01 |
| CaO | 0.03 | 0.04 | 0.02 | 0.04 | 0.02 | 0.03 | 0.03 |
| Al ₂ O ₃ | 0.01 | 0.06 | 0.03 | 0.05 | 0.01 | 0.02 | 0.03 |
| Fe ₂ O ₃ | 0.03 | 0.06 | 0.03 | 0.01 | 0.02 | 0.03 | 0.03 |
| H ₂ O* | 3.13 | 3.48 | 4.87 | 4.58 | 5.31 | 4.43 | 4.30 |
| Total | 97.51 | 97.50 | 97.97 | 98.01 | 99.21 | 98.38 | 98.10 |

Note: H₂O* is calculated by analyzing O by EPMA and assigning the excessive O to H₂O.

3.3. TEM

High-angle annular dark-field image, bright-field TEM image and SAED patterns of moganite are shown in Figure 2. The moganite shows an aggregation of plate-like nanosized crystals with thicknesses of ~5 to 13 nm. The SAED patterns are from a microcrystalline quartz of chert inside the moganite rinds (Figure 2C) and an area dominated by moganite intergrown with nanocrystalline quartz (Figure 2D). Compared to the SAED pattern of nanocrystalline quartz, moganite shows superlattice reflections (Figure 2D) [3]. Streaking reflections result from non-periodic intergrowths of moganite and quartz nanocrystals (or domains).

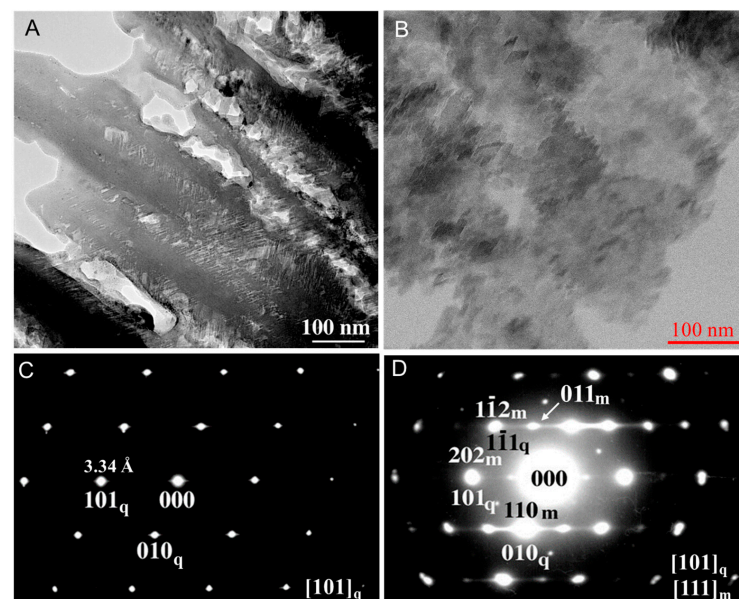


Figure 2. (A) High-angle annular dark-field image of moganite showing moganite nanocrystals. (B) Bright-field TEM image showing feather-like texture of moganite nanocrystals and nano-quartz intergrowth. (C) SAED pattern of microcrystalline quartz grain in a neighboring chert area along the [101]-zone-axis, and (D) the [111]-zone-axis SAED pattern of moganite intergrown with nanocrystalline quartz.

3.4. Neutron/X-ray PDF Analysis

The powder sample of moganite/quartz was treated several times in deionized water to eliminate the co-existing halite and gypsum. The synchrotron XRD pattern of the post-treatment sample shows 80.7(5) wt.% of moganite and 19.3(3) wt.% of quartz (Figure S2). The experimental results of $I(Q)$, $S(Q)$, $F(Q)$ and $G(r)$ from X-ray and neutron scattering of this sample are shown in Supplementary Figures S3 and S4. PDF patterns from 1 to 40 Å are presented in Figure 3. The first major peak at 1.61 Å corresponds to Si–O correlations in silica tetrahedra. The second peak at 2.61–2.62 Å and the third peak at 3.07 Å are related to O–O and Si–Si correlations, respectively, within the corner-sharing SiO_4 tetrahedra.

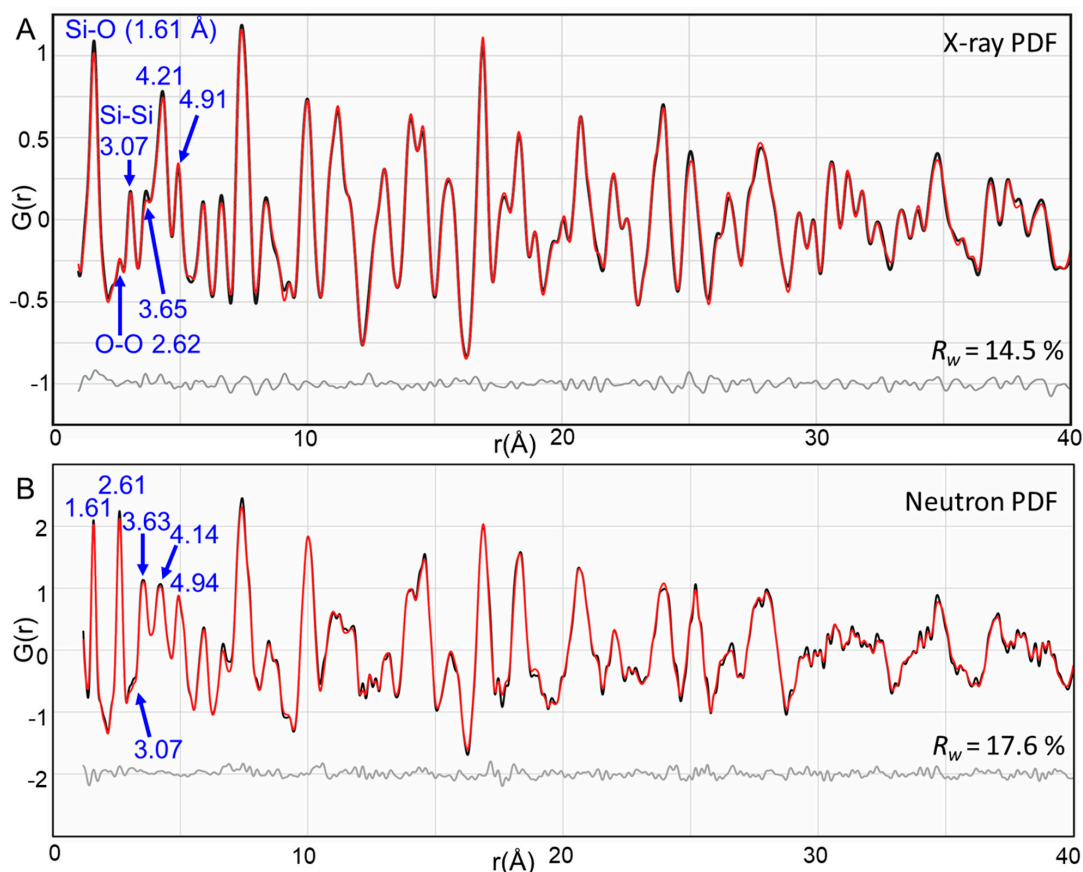


Figure 3. (A) X-ray and (B) neutron pair distribution function (PDF) analysis of X-ray and neutron total scattering data using a mixture model of 80.7 wt.% moganite and 19.3 wt. % quartz from 1 to 40 Å. Black curve: experimental data; red curve: calculated profile; gray curve: differences between the experimental and calculated PDF patterns.

PDF refinement was carried out by fitting the experimental PDF patterns (Figure 3). The initial structures of moganite and quartz for PDF refinement were the refined structures obtained from high-resolution synchrotron XRD data (Table 1). The X-ray PDF refinement mainly focused on determination of ADPs of each atom with the unit cell parameters and atomic coordinates fixed. Based on the differences between experimental and calculated patterns, the results of PDF refinement show an acceptable agreement with the calculated model with a R_w value of 14.5% (Figure 3). For neutron PDF refinement, the unit-cell parameters, atomic coordinates and ADPs of moganite all varied, and the obtained structural parameters are listed in Table 3. The refined quartz structural parameters are listed in Supplementary Table S1. The two obtained sets of structural parameters from X-ray and neutron refinements are generally in good agreement.

Table 3. Unit-cell parameters, atomic coordinates and anisotropic displacement parameters of moganite derived from X-ray and neutron PDF analyses.

| X-ray PDF Analysis: $a = 8.7363 \text{ \AA}$, $b = 4.8688 \text{ \AA}$, $c = 10.7203 \text{ \AA}$ and $\beta = 90.212^\circ$ | | | | | | | | | | |
|----------------------------------------------------------------------------------------------------------------------------------------------|---------|-----------|-----------|-----------|-----------|-----------|-----------|------------|------------|------------|
| Atom | Occ. | x | y | z | U_{11} | U_{22} | U_{33} | U_{12} | U_{13} | U_{23} |
| Si1 | 1 | 0.25 | 0.9731 | 0 | 0.0132(5) | 0.0128(4) | 0.0127(4) | 0 | −0.0003(1) | 0 |
| Si2 | 1 | 0.0089 | 0.2512 | 0.1663 | 0.0165(6) | 0.0184(6) | 0.017(2) | 0.0009(2) | −0.0002(1) | −0.007(3) |
| O1 | 1 | 0.9773 | 0.0651 | 0.2873 | 0.0232(6) | 0.0146(4) | 0.0168(4) | −0.0019(4) | −0.0022(4) | 0.0044(6) |
| O2 | 1 | 0.1683 | 0.1710 | 0.1004 | 0.0171(5) | 0.0215(7) | 0.0167(4) | 0.0064(5) | 0.0043(4) | −0.0025(4) |
| O3 | 1 | 0.8696 | 0.2302 | 0.0676 | 0.0173(5) | 0.0154(5) | 0.0232(8) | −0.0016(3) | −0.0124(3) | −0.0013(2) |
| Neutron PDF Analysis: $a = 8.7357(13) \text{ \AA}$, $b = 4.8675(15) \text{ \AA}$, $c = 10.719(3) \text{ \AA}$ and $\beta = 90.20(3)^\circ$ | | | | | | | | | | |
| Atom | Occ. | x | y | z | U_{11} | U_{22} | U_{33} | U_{12} | U_{13} | U_{23} |
| Si1 | 1 | 0.25 | 0.9733(4) | 0 | 0.0098(5) | 0.0098(4) | 0.0109(5) | 0 | −0.0004(1) | 0 |
| Si2 | 1 | 0.0089(5) | 0.2512(6) | 0.1664(4) | 0.0112(3) | 0.0125(4) | 0.0104(3) | 0.0006(1) | −0.0003(1) | −0.0005(2) |
| O1 | 1.06(1) | 0.9776(5) | 0.0649(6) | 0.2873(4) | 0.0205(5) | 0.0102(3) | 0.0120(5) | −0.0023(2) | −0.0015(3) | 0.0038(5) |
| O2 | 1.06(1) | 0.1681(5) | 0.1712(5) | 0.1005(4) | 0.0161(6) | 0.0212(5) | 0.0129(4) | 0.0035(4) | 0.0019(2) | −0.0014(3) |
| O3 | 1.06(1) | 0.8699(8) | 0.2303(6) | 0.0674(6) | 0.0198(5) | 0.0131(4) | 0.0226(7) | −0.0021(3) | −0.0081(5) | −0.0014(2) |

Since neutrons interact with the nuclei in the sample while X-rays interact with its electrons, neutron scattering is sensitive to light elements such as hydrogen and oxygen. Thus, neutron PDF refinement was also applied to refine the occupancy of O sites in moganite (Table 3), where it is related to the surface OH and silanol group (Si-OH). An excessive occupancy (1.06) of O sites in the moganite structure improved the neutron PDF fitting (R_w value decreases by 1.2%), and the result is shown in Figure S5 and Table S2. Thus, taking into account the excessive oxygen, the chemical formula of moganite is $\text{SiO}_2 \cdot 0.12\text{H}_2\text{O}$ or $\text{SiO}_{1.88}\text{OH}_{0.24}$ (Table 3), which corresponds to 3.5 wt.% of water. The particle size of moganite is estimated as ~6 nm from the long-ranged PDF pattern based on a sudden drop in peak intensities around 5–6 nm range (Figure S6).

4. Discussion

Moganite is a low-temperature precipitate that coexists with fine-grained quartz, halite and gypsum in the late in-filling of cavities, fissures and cracks at ignimbrite flows of the Mogán formation (Figure 1 and Figure S1) [1,2,8]. The emplacement temperature of the pyroclastic flow was above 700 °C, and the volatiles would continuously escape from the flow via fumaroles during cooling [1]. Heaney (1995) suggested that high alkali and sulfate activities play an important role in the formation of moganite. Evaporitic regimes such as arid and alkaline environments were associated with high concentrations of moganite (>30%) [4,10]. Moganite occurs in young rocks with less than ~100 Ma because thermodynamically unstable moganite may transform to quartz or dissolve during silica–water interactions at ambient pressure [2,4,11]. We hypothesize that moganite nanocrystal is stable with respect to quartz in halite-saturated water at low temperature (Figure 4A). The OH[−] sites of moganite confirmed by neutron PDF analysis could adsorb alkali cations such as Na⁺ and K⁺ during its formation. These cations may lower the surface energy of moganite nanocrystals in halite-saturated hypersaline water. In low salinity water, opal instead of moganite forms at low temperature [4,5]. The average size of moganite (~68.6 nm) calculated from XRD refinement is larger than the size from TEM images. The attached moganite nanocrystals with same orientation may contribute to the large average size from XRD refinement. The different methods for studying same mineral often provide different answers. For example, orthoclase shows monoclinic structure in optical microscope and powder XRD; however, TEM shows triclinic nano-domains [40–42]. TEM images also suggest surface-induced nucleation and growth by nanocrystals with the same or similar orientations (Figure 4B).

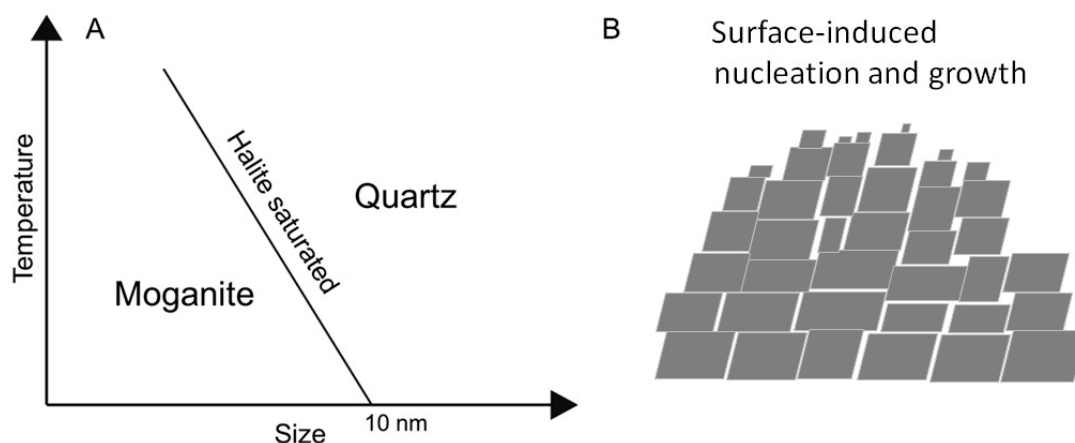


Figure 4. (A) Proposed particle size–temperature phase diagram showing the stability regions of moganite and quartz in halite-saturated water. (B) A schematic diagram showing surface-induced nucleation and growth of moganite nanocrystals with the same or similar orientations.

Determination of the detailed structure of moganite has been difficult because it typically occurs in the form of nano-sized crystals and coexists with other minerals [14,43]. In this case, the application of powder diffraction and related techniques is essential for characterizing the crystal structure [22]. Synchrotron XRD and X-ray/neutron PDF methods provide high-quality structural parameters for moganite (Tables 1 and 3). Our refined unit-cell parameters and bond distances of moganite are in general accordance with those determined by Miehe and Graetsch (1992) [3] and Heaney and Post (2001) [4] (Table 4). However, compared to previous studies, our refined Si(1) and Si(2) bond lengths are much closer to each other, suggesting more regular SiO₄ tetrahedra and position of Si at the centers of regular tetrahedra (Table 4). Overall, the average structures of moganite determined by synchrotron techniques are in good agreement with the previously reported structures.

Table 4. Comparison of unit-cell parameters and bond distances of moganite from different studies.

| | (This Study) | (This Study) | Miehe and Graetsch (1992) | Heaney and Post (2001) |
|--------------------------|--------------|--------------|---------------------------|------------------------|
| Location | Mogán, Spain | Mogán, Spain | Mogán, Spain | Mogán, Spain |
| Source | X-ray | Neutron | X-ray | Neutron |
| Temp | 298 K | 298 K | 298 K | 298 K |
| <i>a</i> (Å) | 8.7363(8) | 8.7357(13) | 8.758(2) | 8.7371(6) |
| <i>b</i> | 4.8688(5) | 4.8675(15) | 4.876(1) | 4.8692(3) |
| <i>c</i> | 10.7203(17) | 10.719(3) | 10.715(2) | 10.7217(7) |
| β (°) | 90.212(13) | 90.20(3) | 90.08(3) | 90.193(9) |
| Volume (Å ³) | 455.99(7) | 455.78(22) | 457.6(2) | 456.13(5) |
| Si(1)-O(2) X 2 | 1.613(5) | 1.614(4) | 1.630(1) | 1.614(4) |
| Si(1)-O(3) X 2 | 1.610(6) | 1.611(7) | 1.603(1) | 1.610(4) |
| Avg. | 1.611(6) | 1.613(5) | 1.617(1) | 1.612(4) |
| Si(2)-O(1) | 1.607(6) | 1.606(6) | 1.601(1) | 1.590(5) |
| Si(2)-O(1) | 1.612(6) | 1.610(6) | 1.622(1) | 1.612(4) |
| Si(2)-O(2) | 1.613(7) | 1.610(5) | 1.596(2) | 1.605(4) |
| Si(2)-O(3) | 1.612(5) | 1.613(9) | 1.635(2) | 1.632(4) |
| Avg. | 1.611(7) | 1.610(7) | 1.614(1) | 1.610(4) |

Although the crystal structures of moganite and quartz are closely related, their XRD and SAED patterns reveal that the atomic arrangement of moganite is different from that of quartz (Figures 1 and 2). The framework structures of quartz and moganite are built by linear silica tetrahedral chains that are connected via bridge tetrahedra (Figure 5). The linear tetrahedral chains are parallel to [010] in moganite and [100] in quartz. The topological difference between the two structures is the position of the tetrahedral bridge which is responsible for the systematic displacements along 1/2 [110] direction at the unit-cell scale (Figure 5) [3,14].

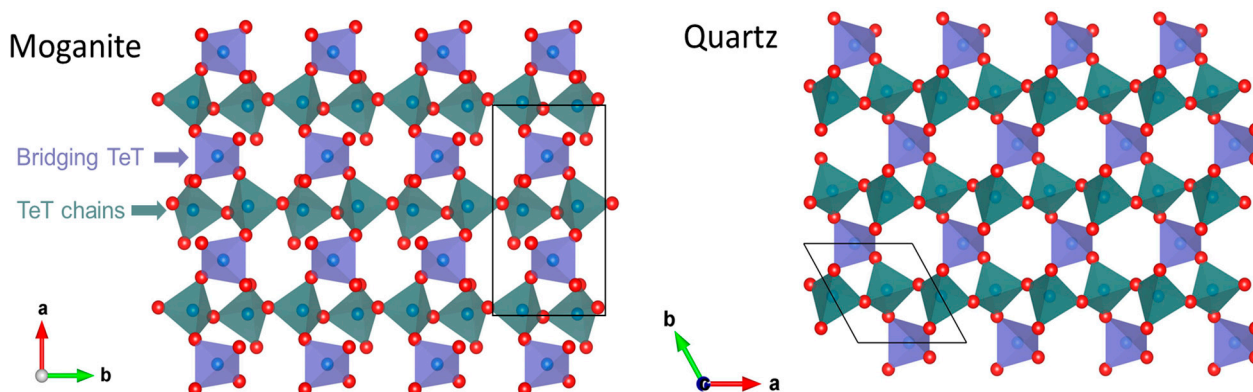


Figure 5. Crystal structures of moganite and quartz projected down the c -axis. Linear tetrahedral chains (green) align along $[010]$ in moganite and $[100]$ in quartz, and are connected via bridging tetrahedra (pale purple).

Moganite structure models from X-ray and neutron PDF analyses are projected along the b -axis (Figure 6). The structure of moganite can be described as alternating slices of right- and left-handed quartz (or unit cell twinning) characterized by the presence of 4- and 6-membered rings of SiO_4 tetrahedra (Figure 5 and Figure S7) [3]. It is known that four-membered rings are present in other silica polymorphs, coesite and opal [44]. Petrovic et al. (1996) suggested that the structural instability of moganite may be associated with the four-membered rings of silica tetrahedra, which are not present in the quartz structure. Other moganite-type phases such as PON [15], $\text{Zn}[\text{BPO}_4(\text{OH})_2]$ [45] and AlPO_4 [16] were synthesized at high-pressure and high-temperature conditions. For example, cristobalite- and quartz-type PON can be transformed into the moganite-type PON after being annealed at 850°C and 2.5 GPa [15]. The unit cell twinning in moganite is similar to that in protoenstatite, whose nanocrystal is stable with respect to enstatite and clinoenstatite at low temperatures [46].

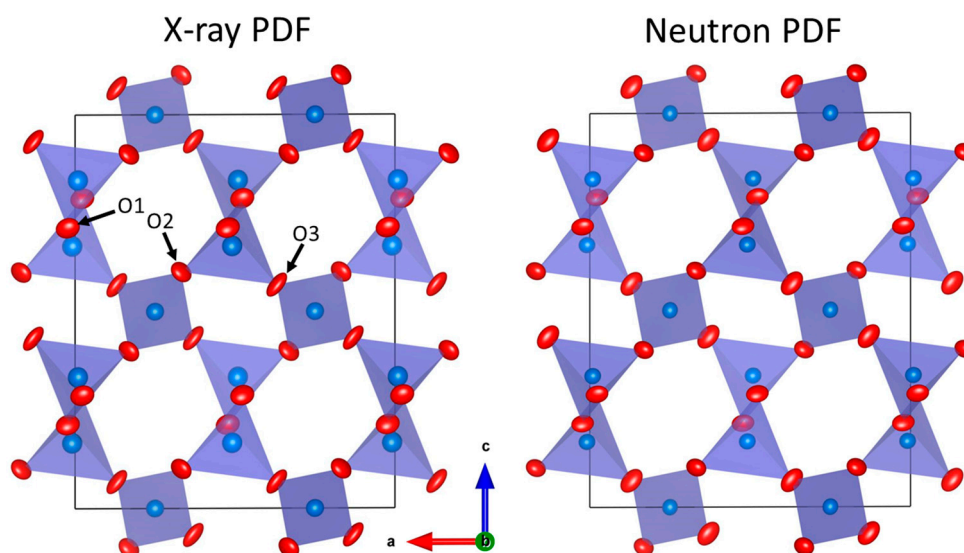


Figure 6. Structural models of moganite derived from X-ray and neutron PDF analyses (Table 2). The models show the displacement ellipsoids of each atom drawn with 80% probability. Blue atoms are silicon, and red atoms are oxygen.

Moganite structure models from X-ray and neutron PDF analyses yielded the displacement ellipsoids of silicon and oxygen atoms (Figure 6). The shape and orientation of the ellipsoids between X-ray and neutron sources are very similar. The anisotropic ellipsoids for the O atoms in moganite extend along the planes perpendicular to the axial direction of corner-sharing SiO_4 tetrahedra, suggesting precession-like motions. Excessive occupancy of O indicates silanol water or Si-OH on surface tetrahedra of moganite nanocrystals. In

In addition, the structure of moganite is compared with that of nanocrystalline quartz from X-ray PDF refinement (this study) and the previously reported quartz structure determined by single-crystal XRD [39] (Supplementary Figure S8). Both moganite and quartz structures show similar shapes and orientations of their anisotropic ellipsoids (Supplementary Figure S8). The nanocrystalline quartz shows relatively larger unit cell and ADP parameters than those in bulk quartz (Table 1 and Supplementary Table S1), which can be attributed to surface relaxation of quartz nanocrystals. Therefore, our results confirm that X-ray and neutron PDF techniques are powerful to characterize the stoichiometry (Si/O ratio) and ADPs of moganite and provide high-quality crystalline structural information.

5. Conclusions

The results of this study have important implications for how to determine the average and local structure of natural moganite. The combined synchrotron XRD and X-ray/Neutron PDF analysis is a powerful tool to obtain high-quality structural parameters. Rietveld analysis of Bragg peaks from synchrotron XRD determines the average structure of moganite nanocrystals. The unit-cell parameters and bond distances of the refined moganite structure show consistency with the previously reported structures. On the other hand, X-ray and neutron PDF methods can provide the local structure of moganite including its ADPs. The shapes and orientations of anisotropic ellipsoids of atoms in the refined moganite structure show similar tendencies to those of the quartz structure. Neutron PDF also confirms the occupancy of O sites, suggesting surface OH and silanol (Si-OH) in moganite, which are previously determined by IR and NMR studies [17–19]. In nature, the monovalent cations adsorbed on moganite can lower its surface energy, which can explain why moganite nanomineral is stable with respect to quartz in halite-saturate hypersaline water. In short, the results from this combined approach can provide high-quality structural parameters of fine-grained minerals such as moganite and quartz nanocrystals. This approach can be used as an alternative means for refining structures of crystals that are not large enough for single-crystal XRD measurements. The approach will be useful for the structural determination of other submicron sized crystals and nanominerals formed in geological environments.

Supplementary Materials: The following are available online at <https://www.mdpi.com/2075-163X/11/3/272/s1>, Figure S1: Moganite coexisting with microcrystalline quartz collected from cherts in the ignimbrite lava flows of the Mogán formation, Figure S2: Synchrotron XRD pattern of the sample without halite and gypsum, Figure S3: Experimental results of X-ray scattering patterns of I(Q), S(Q), F(Q), and PDF, Figure S4: Time-of-flight neutron scattering profiles, S(Q), and PDF, Figure S5: PDF refinement of neutron PDF patterns using a two-structure models of moganite (full occupancy and partial occupancy of O sites), Figure S6: Neutron PDF patterns of moganite and Si standard from 0.5 to 100 Å, Figure S7: Crystal structures of the moganite and quartz from X-ray PDF refinement, Figure S8: Crystal structures of moganite, nano-crystalline quartz, and bulk quartz projected along the *a*- and *c*-axes, Table S1: Unit-cell parameters, atomic coordinates, and anisotropic displacement parameters of nano-crystalline quartz from X-ray and neutron PDF refinement compared with previously reported quartz structure, Table S2: Unit-cell parameters, atomic coordinates, and anisotropic displacement parameters of two structure models of moganite (full occupancy and partial occupancy of O sites) determined by neutron PDF refinement.

Author Contributions: Conceptualization, H.X. (Huifang Xu); methodology, H.X. (Huifang Xu), S.L., J.N.; software, S.L.; validation, H.X. (Huifang Xu), H.X. (Hongwu Xu) and J.N.; formal analysis, S.L., H.X. (Huifang Xu); investigation, S.L., H.X. (Huifang Xu); resources, H.X. (Huifang Xu), H.X. (Hongwu Xu); data curation, H.X. (Huifang Xu), H.X. (Hongwu Xu), S.L., J.N.; writing—original draft preparation, S.L.; writing—review and editing, H.X. (Huifang Xu), H.X. (Hongwu Xu), J.N.; visualization, S.L.; supervision, H.X. (Huifang Xu); project administration, H.X. (Huifang Xu); funding acquisition, H.X. (Huifang Xu). S.L. carried out the experiment and drafted the manuscript; H.X. (Huifang Xu) conceived the idea; all the co-authors contributed to manuscript writing. All authors have read and agreed to the published version of the manuscript.

Funding: This research was funded by NASA Astrobiology Institute, grant number NNA13AA94A.

Institutional Review Board Statement: Not applicable.

Informed Consent Statement: Not applicable.

Data Availability Statement: The data presented in this study are available on request from the corresponding author.

Acknowledgments: The authors acknowledge the critical reviews and constructive suggestions from the three anonymous reviewers. Synchrotron X-ray data were collected at the Advanced Photon Source, a U.S. Department of Energy (DOE) Office of Science User Facility, operated for the DOE Office of Science by Argonne National Laboratory under Contract No. DE-AC02-06CH11357. A portion of this research used resources at the SNS, a DOE Office of Science User Facility operated by the Oak Ridge National Laboratory. This work was partly supported by the Laboratory Directed Research and Development (LDRD) program at Los Alamos National Laboratory (LANL). LANL, an affirmative action/equal opportunity employer, managed by Triad National Security Administration of the U.S. Department of Energy under contract number 89233218CNA000001.

Conflicts of Interest: The authors declare no conflict of interest.

References

1. Flörke, O.; Jones, J.; Schmincke, H.U. A new microcrystalline silica from Gran Canaria. *Z. Kristallogr. Krist.* **1976**, *143*, 156–165. [[CrossRef](#)]
2. Heaney, P.J.; Post, J.E. The widespread distribution of a novel silica polymorph in microcrystalline quartz varieties. *Science* **1992**, *255*, 441–443. [[CrossRef](#)]
3. Mieke, G.; Graetsch, H. Crystal structure of moganite: A new structure type for silica. *Eur. J. Mineral.* **1992**, *4*, 693–706. [[CrossRef](#)]
4. Heaney, P.J. Moganite as an indicator for vanished evaporites; a testament reborn? *J. Sediment. Res.* **1995**, *65*, 633–638.
5. Petrovic, I.; Heaney, P.J.; Navrotsky, A. Thermochemistry of the new silica polymorph moganite. *Phys. Chem. Miner.* **1996**, *23*, 119–126. [[CrossRef](#)]
6. Götze, J.; Nasdala, L.; Kleeberg, R.; Wenzel, M. Occurrence and distribution of “moganite” in agate/chalcedony: A combined micro-Raman, Rietveld, and cathodoluminescence study. *Contrib. Mineral. Petrol.* **1998**, *133*, 96–105. [[CrossRef](#)]
7. Rodgers, K.; Cressey, G. The occurrence, detection and significance of moganite (SiO₂) among some silica sinters. *Mineral. Mag.* **2001**, *65*, 157–167. [[CrossRef](#)]
8. Flörke, O.; Flörke, U.; Giese, U. Moganite. A new microcrystalline silica-mineral. *Neues Jahrb. Mineral. Abhandlungen* **1984**, *149*, 325–336.
9. Xu, H.; Buseck, P.R.; Gufeng, L. HRTEM investigation of microstructures in length-slow chalcedony. *Am. Mineral.* **1998**, *83*, 542–545. [[CrossRef](#)]
10. Parthasarathy, G.; Kunwar, A.C.; Srinivasan, R. Occurrence of moganite-rich chalcedony in Deccan flood basalts, Killari, Maharashtra, India. *Eur. J. Mineral.* **2001**, *13*, 127–134. [[CrossRef](#)]
11. Gislason, S.R.; Heaney, P.J.; Oelkers, E.H.; Schott, J. Kinetic and thermodynamic properties of moganite, a novel silica polymorph. *Geochim. Cosmochim. Acta* **1997**, *61*, 1193–1204. [[CrossRef](#)]
12. Moxon, T.; Ríos, S. Moganite and water content as a function of age in agate: An XRD and thermogravimetric study. *Eur. J. Mineral.* **2004**, *16*, 269–278. [[CrossRef](#)]
13. Kayama, M.; Tomioka, N.; Ohtani, E.; Seto, Y.; Nagaoka, H.; Götze, J.; Miyake, A.; Ozawa, S.; Sekine, T.; Miyahara, M. Discovery of moganite in a lunar meteorite as a trace of H₂O ice in the Moon’s regolith. *Sci. Adv.* **2018**, *4*, eaar4378. [[CrossRef](#)] [[PubMed](#)]
14. Heaney, P.J.; Post, J.E. Evidence for an *I 2/a* to *Imab* phase transition in the silica polymorph moganite at ~570 K. *Am. Mineral.* **2001**, *86*, 1358–1366. [[CrossRef](#)]
15. Chateau, C.; Haines, J.; Leger, J.-M.; LeSauze, A.; Marchand, R. A moganite-type phase in the silica analog phosphorus oxynitride. *Am. Mineral.* **1999**, *84*, 207–210. [[CrossRef](#)]
16. Kanzaki, M.; Xue, X. Structural characterization of moganite-type AlPO₄ by NMR and powder X-ray diffraction. *Inorg. Chem.* **2012**, *51*, 6164–6172. [[CrossRef](#)] [[PubMed](#)]
17. Graetsch, H.; Flörke, O.; Mieke, G. Structural defects in microcrystalline silica. *Phys. Chem. Miner.* **1987**, *14*, 249–257. [[CrossRef](#)]
18. Mieke, G. Die monokline Kristallstruktur des SiO₂ Minerals Moganit. *Z. Kristallogr. Krist.* **1988**, *182*, 183–184.
19. Zhang, M.; Moxon, T. In situ infrared spectroscopic studies of OH, H₂O and CO₂ in moganite at high temperatures. *Eur. J. Mineral.* **2012**, *24*, 123–131. [[CrossRef](#)]
20. Zhang, M.; Moxon, T. Infrared absorption spectroscopy of SiO₂-moganite. *Am. Mineral.* **2014**, *99*, 671–680. [[CrossRef](#)]
21. Schmidt, P.; Bellot-Gurlet, L.; Léa, V.; Sciau, P. Moganite detection in silica rocks using Raman and infrared spectroscopy. *Eur. J. Mineral.* **2013**, *25*, 797–805. [[CrossRef](#)]
22. Lee, S.; Xu, H. Using complementary methods of synchrotron radiation powder diffraction and pair distribution function to refine crystal structures with high quality parameters—A Review. *Minerals* **2020**, *10*, 124. [[CrossRef](#)]

23. Lee, S.; Xu, H. Using powder XRD and pair distribution function to determine anisotropic atomic displacement parameters of orthorhombic tridymite and tetragonal cristobalite. *Acta Crystallogr. Sect. B Struct. Sci. Cryst. Eng. Mater.* **2019**, *75*, 160–167. [[CrossRef](#)] [[PubMed](#)]
24. Egami, T.; Billinge, S.J. *Underneath the Bragg Peaks: Structural Analysis of Complex Materials*, 2nd ed.; Elsevier: Oxford, UK, 2012; pp. 10–32.
25. Xu, H.; Heaney, P.J.; Beall, G.H. Phase transitions induced by solid solution in stuffed derivatives of quartz: A powder synchrotron XRD study of the $\text{LiAlSiO}_4\text{-SiO}_2$ join. *Am. Mineral.* **2000**, *85*, 971–979. [[CrossRef](#)]
26. Xu, H.; Navrotsky, A.; Balmer, M.L.; Su, Y. Crystal chemistry and phase transitions in substituted pollucites along the $\text{CsAlSi}_2\text{O}_6\text{-CsTiSi}_2\text{O}_{6.5}$ join: A powder synchrotron X-ray diffractometry study. *J. Am. Ceram. Soc.* **2002**, *85*, 1235–1242. [[CrossRef](#)]
27. Xu, H.; Zhao, Y.; Zhang, J.; Hickmott, D.D.; Daemen, L.L. In situ neutron diffraction study of deuterated portlandite $\text{Ca}(\text{OD})_2$ at high pressure and temperature. *Phys. Chem. Miner.* **2007**, *34*, 223–232. [[CrossRef](#)]
28. Xu, H.; Zhao, Y.; Vogel, S.C.; Hickmott, D.D.; Daemen, L.L.; Hartl, M.A. Thermal expansion and decomposition of jarosite: A high-temperature neutron diffraction study. *Phys. Chem. Miner.* **2010**, *37*, 73–82. [[CrossRef](#)]
29. Lee, S.; Xu, H.; Xu, W.; Sun, X. The structure and crystal chemistry of vernadite in ferromanganese crusts. *Acta Crystallogr. Sect. B Struct. Sci. Cryst. Eng. Mater.* **2019**, *75*, 591–598. [[CrossRef](#)] [[PubMed](#)]
30. Trueblood, K.; Bürgi, H.B.; Burzlaff, H.; Dunitz, J.; Gramaccioli, C.; Schulz, H.; Shmueli, U.; Abrahams, S. Atomic displacement parameter nomenclature. Report of a subcommittee on atomic displacement parameter nomenclature. *Acta Crystallogr. Sect. A Found. Crystallogr.* **1996**, *52*, 770–781. [[CrossRef](#)]
31. Graetsch, H.; Topalovic, I.; Gies, H. NMR spectra of moganite and chalcedony. *Eur. J. Mineral.* **1994**, *6*, 459–464. [[CrossRef](#)]
32. Toby, B.H.; Von Dreele, R.B. GSAS-II: The genesis of a modern open-source all purpose crystallography software package. *J. Appl. Crystallogr.* **2013**, *46*, 544–549. [[CrossRef](#)]
33. Kihara, K. An X-ray study of the temperature dependence of the quartz structure. *Eur. J. Mineral.* **1990**, *2*, 63–78. [[CrossRef](#)]
34. Comodi, P.; Nazzareni, S.; Zanazzi, P.F.; Speziale, S. High-pressure behavior of gypsum: A single-crystal X-ray study. *Am. Mineral.* **2008**, *93*, 1530–1537. [[CrossRef](#)]
35. Finger, L.; King, H. A revised method of operation of the single-crystal diamond cell and refinement of the structure of NaCl at 32 kbar. *Am. Mineral.* **1978**, *63*, 337–342.
36. Juhás, P.; Davis, T.; Farrow, C.L.; Billinge, S.J. PDFgetX3: A rapid and highly automatable program for processing powder diffraction data into total scattering pair distribution functions. *J. Appl. Crystallogr.* **2013**, *46*, 560–566. [[CrossRef](#)]
37. Farrow, C.; Juhas, P.; Liu, J.; Bryndin, D.; Božin, E.; Bloch, J.; Proffen, T.; Billinge, S. PDFfit2 and PDFgui: Computer programs for studying nanostructure in crystals. *J. Phys. Condens. Matter* **2007**, *19*, 335219. [[CrossRef](#)] [[PubMed](#)]
38. Peterson, P.; Gutmann, M.; Proffen, T.; Billinge, S. PDFgetN: A user-friendly program to extract the total scattering structure factor and the pair distribution function from neutron powder diffraction data. *J. Appl. Crystallogr.* **2000**, *33*, 1192. [[CrossRef](#)]
39. Antao, S.M.; Hassan, I.; Wang, J.; Lee, P.L.; Toby, B.H. State-of-the-art high-resolution powder X-ray diffraction (HRPXRD) illustrated with Rietveld structure refinement of quartz, sodalite, tremolite, and meionite. *Can. Mineral.* **2008**, *46*, 1501–1509. [[CrossRef](#)]
40. Xu, H.; Jin, S.; Lee, S.; Hobbs, F.W. Nano-phase $\text{KNa}(\text{Si}_6\text{Al}_2)\text{O}_{16}$ in adularia: A new member in the alkali feldspar series with ordered K–Na distribution. *Minerals* **2019**, *9*, 649. [[CrossRef](#)]
41. Ribbe, P.H. Aluminium-silicon order in feldspars; domain textures and diffraction patterns. In *Feldspar Mineralogy*; De Gruyter: Berlin, Germany, 1983; Volume 2, pp. 21–55.
42. Xu, H.; Veblen, D.R.; Buseck, P.; Ramakrishna, B.L. TEM and SFM of exsolution and twinning in an alkali feldspar. *Am. Mineral.* **2000**, *85*, 509–513. [[CrossRef](#)]
43. Hantsch, U.; Winkler, B.R.; Pickard, C.J.; Warren, M.C.; Milman, V.; Mauri, F. Theoretical investigation of moganite. *Eur. J. Mineral.* **2005**, *17*, 21–30. [[CrossRef](#)]
44. Lee, S.; Cai, J.; Jin, S.; Zhang, D.; Thevamaran, R.; Xu, H. Coesite formation at low pressure during supersonic microprojectile impact of opal. *ACS Earth Space Chem.* **2020**, *4*, 1291–1297. [[CrossRef](#)]
45. Huang, Y.X.; Prots, Y.; Kniep, R. $\text{Zn}[\text{BPO}_4(\text{OH})_2]$: A zinc borophosphate with the rare moganite-type uopology. *Chem. Eur. J.* **2008**, *14*, 1757–1761. [[CrossRef](#)] [[PubMed](#)]
46. Xu, H.; Hill, T.R.; Konishi, H.; Farfan, G. Protoenstatite: A new mineral in Oregon sunstones with “watermelon” colors. *Am. Mineral.* **2017**, *102*, 2146–2149. [[CrossRef](#)]